

Mechanism of nucleotide discrimination by the translesion synthesis polymerase Rev1

Tyler M. Weaver^{1,2}, Timothy H. Click³, Thu H. Khoang^{1,2}, M. Todd Washington⁴, Pratul K. Agarwal³✉ & Bret D. Freudenthal^{1,2}✉

Rev1 is a translesion DNA synthesis (TLS) polymerase involved in the bypass of adducted-guanine bases and abasic sites during DNA replication. During damage bypass, Rev1 utilizes a protein-template mechanism of DNA synthesis, where the templating DNA base is evicted from the Rev1 active site and replaced by an arginine side chain that preferentially binds incoming dCTP. Here, we utilize X-ray crystallography and molecular dynamics simulations to obtain structural insight into the dCTP specificity of Rev1. We show the Rev1 R324 protein-template forms sub-optimal hydrogen bonds with incoming dTTP, dGTP, and dATP that prevents Rev1 from adopting a catalytically competent conformation. Additionally, we show the Rev1 R324 protein-template forms optimal hydrogen bonds with incoming rCTP. However, the incoming rCTP adopts an altered sugar pucker, which prevents the formation of a catalytically competent Rev1 active site. This work provides novel insight into the mechanisms for nucleotide discrimination by the TLS polymerase Rev1.

¹Department of Biochemistry and Molecular Biology, University of Kansas Medical Center, Kansas City, Kansas 66160, USA. ²Department of Cancer Biology, University of Kansas Medical Center, Kansas City, Kansas 66160, USA. ³Department of Physiological Sciences and High-Performance Computing Center, Oklahoma State University, Stillwater, Oklahoma 74048, USA. ⁴Department of Biochemistry and Molecular Biology, University of Iowa, Iowa City, IA 52242, USA. ✉email: pratul.agarwal@okstate.edu; bfreudenthal@kumc.edu

DNA polymerases are tasked with the faithful replication of genomic DNA during each cycle of cell division^{1–3}. The faithful replication of the genome requires DNA polymerases bind and add the correct incoming deoxynucleotide triphosphate (dNTP) to the end of a growing DNA primer strand. Importantly, the correct nucleotide must be chosen amongst a pool of excess incorrect nucleotides that contain either the wrong DNA nucleobase (i.e. base) or the wrong sugar moiety (e.g. ribonucleotide triphosphates, rNTP). DNA polymerases use an induced-fit mechanism for selecting and incorporating the correct dNTP^{4–8}. In the induced-fit mechanism, the DNA polymerase undergoes a conformational change during dNTP binding, which allows for sampling of proper Watson-Crick base pairing with the templating DNA base. When the correct nucleotide is bound the 3'-OH of the primer terminus, P α of the incoming nucleotide, and catalytic metal are in the proper orientation for catalysis within the active site⁹. If the incorrect nucleotide is bound, the sub-optimal base pairing between the incoming nucleotide and templating DNA base leads to conformational changes in the active site that are not conducive to catalysis^{9,10}. In addition to DNA base fidelity, DNA polymerases also possess mechanisms to maintain sugar fidelity. This includes an active site bulky aromatic steric gate residue that clashes with the 2'-OH of the incoming ribonucleotide triphosphate^{11,12}. In some cases, DNA polymerases also use a polar filter residue that locks the C2' of the incoming ribonucleotide near the steric gate residue¹³. Ultimately, the ability to bind the correct incoming nucleotide enables DNA polymerases to faithfully replicate and repair genomic DNA.

Rev1 is a specialized Y-family DNA polymerase involved in translesion DNA synthesis (TLS), replication of G4-quadruplex DNA^{14–16}, replication-induced gap filling¹⁷, and somatic hypermutation¹⁸. Rev1 is best known for its functions during TLS, where it acts as both a scaffolding component and a TLS DNA polymerase^{19–23}. The DNA synthesis activity of Rev1 is important for the bypass of adducted-guanine bases and abasic sites, which otherwise stall replicative DNA polymerases and potentially collapse replication forks. The initial characterization of the Rev1 DNA synthesis activity observed a significant preference for cytosine insertion, irrespective of the templating DNA base identity^{24–28}. Subsequent structural studies revealed the preference for cytosine insertion is due to the use of an unusual protein-template mechanism^{29–34}. In the protein-template mechanism, the templating DNA base is evicted from the Rev1 active site and is replaced by an arginine side chain residue (Fig. 1). This arginine side chain forms two hydrogen bonds with

an incoming dCTP, which is thought to enable the preferentially insertion of dCTP. Notably, Rev1 is the only DNA polymerase known to use an amino-acid side chain to encode for an incoming nucleotide, instead of a templating DNA base². Additionally, Rev1 does not undergo large conformational changes upon incoming nucleotide binding. This makes Rev1 an interesting system to study mechanisms of nucleotide discrimination by a non-classical DNA polymerase.

Several groups have studied the base and sugar discrimination of Rev1 using enzyme kinetics (Supplementary Table 1)^{24–28,35,36}. With respect to base discrimination, human Rev1 preferentially incorporates a dCTP opposite a template G^{36,37}. dGTP and dTTP are incorporated opposite G with 260- and 140-fold reduced relative catalytic efficiency ($k_{\text{pol}}/K_{\text{d}}$), respectively, relative to dCTP incorporation³⁷. Rev1 incorporates dATP opposite a template G with a 14,000-fold reduced relative catalytic efficiency ($k_{\text{pol}}/K_{\text{d}}$) relative to dCTP incorporation³⁷. With respect to sugar discrimination, Rev1 preferentially incorporates rCTP opposite a templating G with a 280-fold reduced relative catalytic efficiency ($k_{\text{pol}}/K_{\text{d}}$) compared to dCTP³⁷. The structural basis for the dCTP specificity of Rev1 has been unclear, largely owing to the absence of structural information about the enzyme-substrate complexes with sub-optimal incoming NTPs. Here, we utilize X-ray crystallography and molecular dynamics (MD) simulations to obtain insight into the structure and dynamics of Rev1 interacting with different incoming NTPs, which explains the structural basis for Rev1 dCTP specificity.

Results

Structural basis for Rev1 DNA base specificity. To obtain structural insight for the interaction of Rev1 and an incoming dTTP, we determined a ternary complex (Rev1/DNA/dNTP) structure of Rev1 with an incoming dTTP. To accomplish this, Rev1 was crystallized in complex with a primer-template DNA generating Rev1/DNA binary complex crystals. The Rev1/DNA binary complex crystals were then transferred to a cryoprotectant containing dTTP and CaCl₂ to generate Rev1-dTTP ternary complex crystals. Importantly, Ca²⁺ permits incoming nucleotide binding but does not facilitate catalysis *in crystallo*³⁴. The resulting Rev1/DNA/dTTP ternary complex crystal diffracted to 1.70 Å and was in space group P2₁2₁2₁ (Supplementary Table 2).

The overall structure of the Rev1-dTTP ternary complex is similar to the Rev1-dCTP ternary complex structure (RMSD = 0.228 Å), including the evicted templating guanine base, the R324 protein template, and Rev1 active site side chains

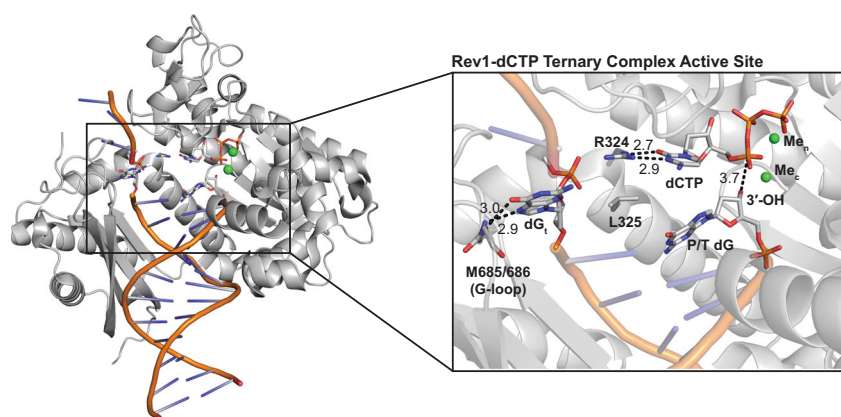


Fig. 1 Rev1/DNA/dCTP ternary complex structure. An overall structure (left) and active site closeup (right) of the Rev1/DNA/dCTP ternary complex (PDB:6X6Z). Key protein and DNA residues are shown as gray sticks and labeled. The nucleotide binding (Me_n) and catalytic (Me_c) metals are shown as green spheres.

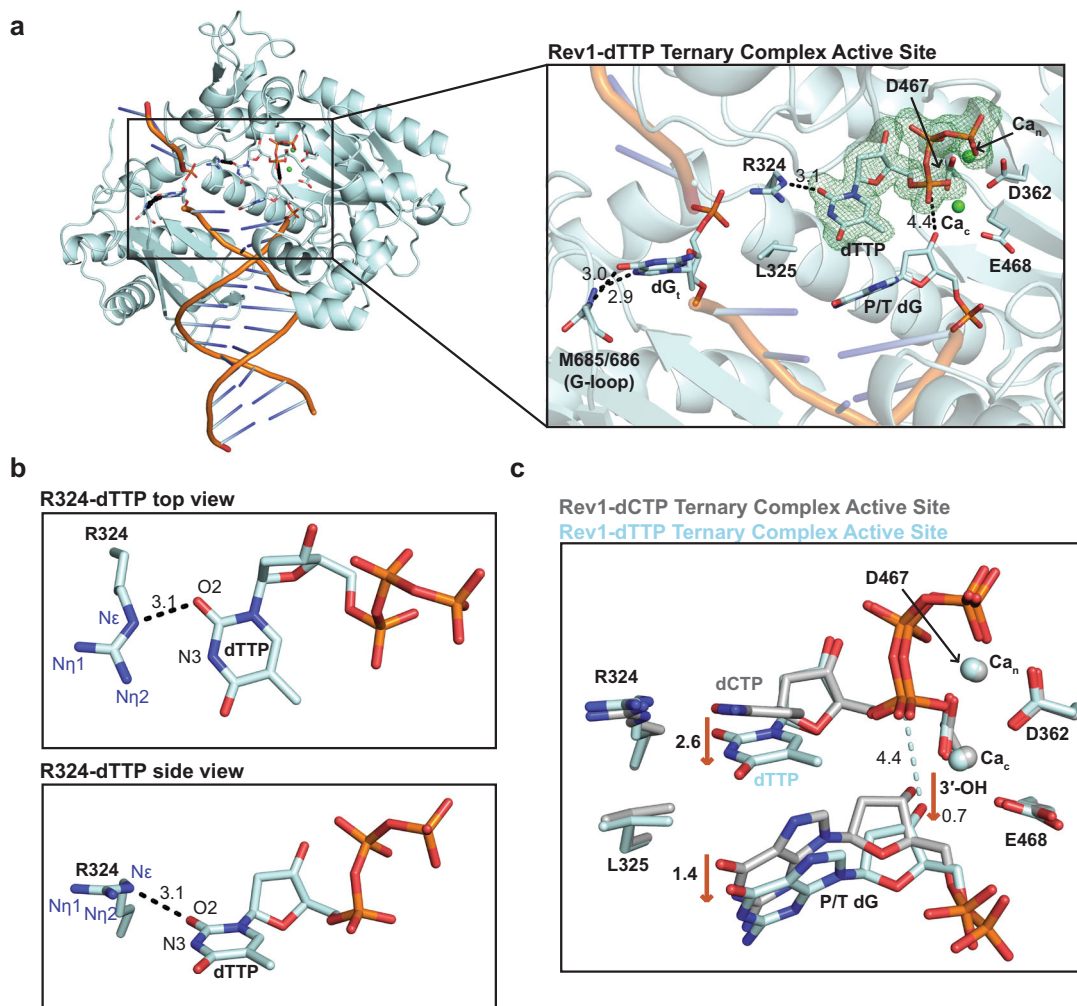


Fig. 2 Rev1/DNA/dTTP ternary complex structure. **a** An overall structure (left) and active site close-up (right) of the Rev1/DNA/dTTP ternary complex. Key protein and DNA residues are shown as blue sticks. The nucleotide binding (Ca_n) and catalytic (Ca_c) metals are shown as green spheres. A Polder OMIT map contoured at $\sigma = 3.0$ for the incoming dTTP is shown as a green mesh. **b** Two focused views of the hydrogen bonds formed between Rev1 R324 and the incoming dTTP. Hydrogen bonds are shown as black dashed lines and hydrogen bonding distances are labeled. **c** An overlay of the Rev1/DNA/dTTP ternary complex (light blue sticks) and Rev1/DNA/dCTP ternary complex (gray sticks). Red arrows and the respective distances (Å) highlight key active site differences between the two structures. The nucleotide binding (Ca_n) and catalytic (Ca_c) metals are shown as spheres.

(Supplementary Fig. 1). However, major differences were seen in the conformation of the incoming dTTP and the primer terminal dG base (Fig. 2 and Supplementary Fig. 1). Figure 2a shows the overall Rev1-dTTP ternary complex structure and a close-up of the Rev1 active site. The Rev1-dTTP ternary complex contains the incoming dTTP and both nucleotide (Ca_n) and catalytic (Ca_c) calcium ions (Fig. 2a). The incoming dTTP is coordinated by the R324 through a single non-planar hydrogen bond between the $O2$ of the Watson-Crick edge and the $N\epsilon$ of R324 (Fig. 2b). Notably, the position of the dTTP ribose sugar and triphosphate group are in a similar conformation to that seen in the Rev1-dCTP ternary complex structure (Fig. 2c). Structural superimposition of the Rev1-dTTP and Rev1-dCTP ternary complex structures revealed several changes to the Rev1 active site with implications for dTTP insertion (Fig. 2c). The non-planar R324-dTTP interaction leads to a 2.6 Å movement in the dTTP base towards the primer terminal dG. To accommodate the dTTP, the primer terminal dG moves 1.4 Å downward from the conformation seen in the Rev1-dCTP ternary complex structure. This brings the 3'-OH of the primer terminal dG 4.4 Å away from Pa of the incoming dTTP, which is ~ 1 Å increase compared to the Rev1-dCTP ternary complex structure (Figs. 1 and 2c). This increase shifts the 3'-OH

out of a catalytically competent conformation to support nucleophilic attack on the Pa of the incoming dTTP. Together, the loss of a single hydrogen bond between R324 and the dTTP and the altered conformation of the primer terminal dG 3'-OH explains the observed reduction in nucleotide binding and catalysis that was previously described for Rev1 insertion of dTTP (Supplementary Table 1)^{36,37}.

To obtain structural insight into Rev1 interacting with an incoming dGTP, we determined a 2.0 Å structure of the Rev1/DNA/dGTP ternary complex (Supplementary Table 2). The overall Rev1-dGTP ternary complex structure is very similar to the Rev1-dCTP ternary complex (RMSD = 0.306 Å, Supplementary Fig. 2). However, major alterations to the Rev1 active site were observed including the conformation of the dGTP and subtle conformational changes in the primer terminal dG base were observed (Fig. 3 and Supplementary Fig. 2). Figure 3a shows the overall Rev1-dGTP ternary complex structure and a close-up of the Rev1 active site, which contains the incoming dGTP and nucleotide Ca_n ion. Interestingly, the catalytic Ca_c was not observed and the binding site was instead taken up by a water molecule. In the Rev1-dGTP ternary complex structure, the dGTP base adopts a Hoogsteen conformation, instead of the traditional

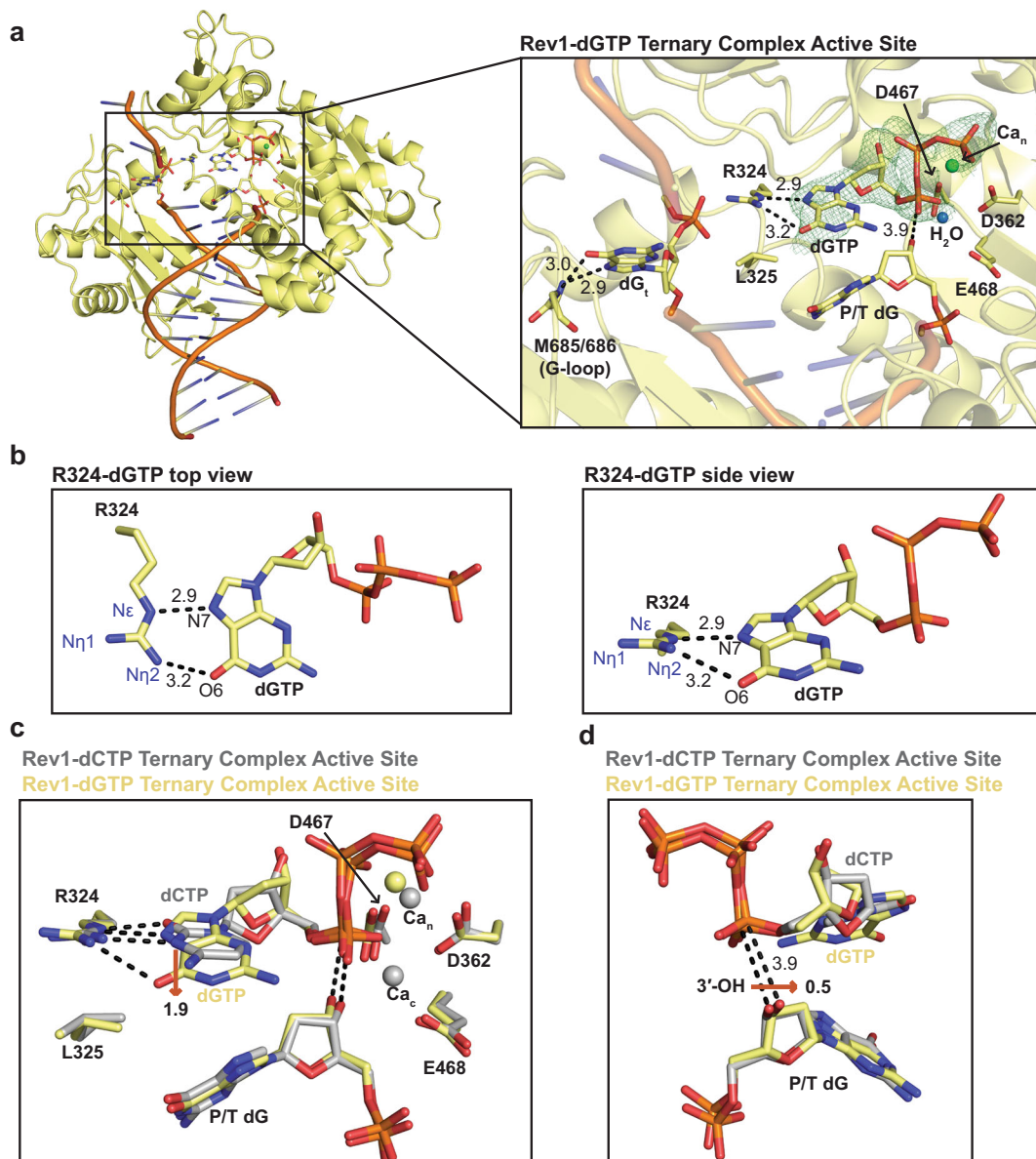


Fig. 3 Rev1/DNA/dGTP ternary complex structure. **a** An overall structure (left) and active site closeup (right) of the Rev1/DNA/dGTP ternary complex. Key protein and DNA residues are shown as yellow sticks. The nucleotide binding (Ca_n) metal and water molecule that replaces the catalytic metal (Ca_c) are shown as a green and blue sphere, respectively. A Polder OMIT map contoured at $\sigma = 3.0$ for the incoming dGTP is shown as a green mesh. **b** Two focused views of the hydrogen bonds formed between Rev1 R324 and the incoming dGTP. Hydrogen bonds are shown as black dashed lines and hydrogen bonding distances (\AA) are labeled. **c** An overlay of the Rev1/DNA/dGTP ternary complex (yellow sticks) and Rev1/DNA/dCTP ternary complex (gray sticks) showing differences in the dNTP bases. Red arrows and distances (\AA) highlight key differences between the two structures. The nucleotide binding (Ca_n) and catalytic (Ca_c) metals are shown as spheres. **d** An overlay of the Rev1/DNA/dGTP ternary complex (yellow sticks) and Rev1/DNA/dCTP ternary complex (gray sticks) showing differences in the position of the primer terminal dG 3'-OH. Red arrows and the respective distances (\AA) show the movement of the primer terminal dG 3'-OH between the two structures.

Watson-Crick conformation. In this conformation, the Hoogsteen edge of the dGTP faces the R324 protein-temple. The N_ϵ and N_η of R324 form two non-planar hydrogen bonds with the N7 and O6 of the dGTP Hoogsteen edge (Fig. 3b). Interestingly, the dGTP ribose adopts a non-canonical $\text{C1}'$ -exo sugar pucker, which is different than the $\text{C3}'$ -endo sugar pucker seen with incoming dCTP (Fig. 3a, c). Despite the differences in DNA base and sugar conformations, the triphosphate group of the dGTP is anchored in the Rev1 active site in similar conformation as incoming dCTP (Fig. 3c, d). Structural superimposition of the Rev1-dGTP and Rev1-dCTP ternary complex structures revealed additional changes to the Rev1 active site with implications for catalysis

(Fig. 3c, d). The non-planar interactions between the dGTP and R324 lead to a 1.9 \AA movement of the dGTP base towards the primer terminal dG. This conformational change leads to a subtle 0.5 \AA movement in the 3'-OH of the primer terminal dG distal to the Pa of the incoming dGTP (Fig. 3d). In this conformation, the 3'-OH is 3.9 \AA from the Pa of the incoming dGTP, which is slightly longer than the 3.7 \AA seen in the Rev1-dCTP ternary complex (Fig. 3a). Ultimately, the Hoogsteen conformation of the dGTP explains the reduction in nucleotide binding, while the subtle movement in the 3'-OH distal to the Pa can explain the minor decrease in catalysis that was previously described for Rev1 insertion of dGTP (Supplementary Table 1)^{36,37}.

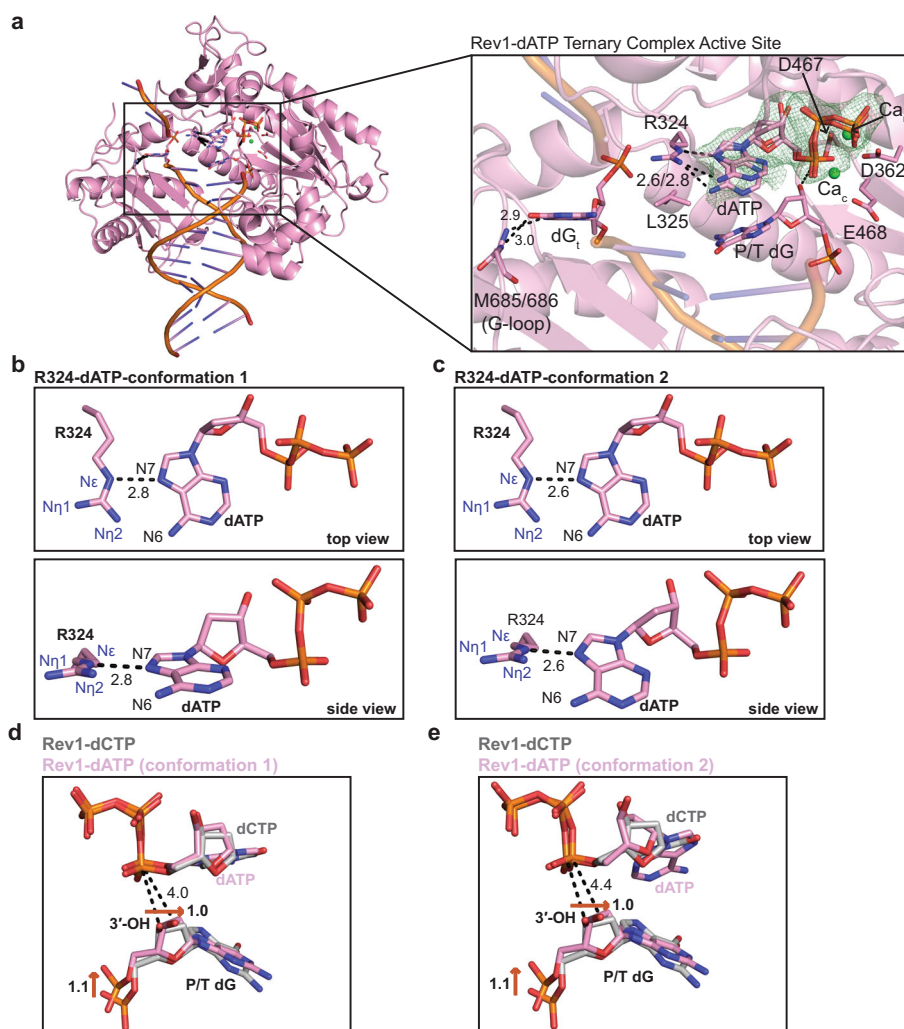


Fig. 4 Rev1/DNA/dATP ternary complex structure. **a** An overall structure (left) and active site close-up (right) of the Rev1/DNA/dATP ternary complex. Key protein and DNA residues are shown as pink sticks. The nucleotide binding (Ca_n) and catalytic (Ca_c) metals are shown as green spheres. A Polder OMIT map contoured at $\sigma = 3.0$ for the incoming dATP is shown as a green mesh. **b** Two focused views of the hydrogen bonds formed between Rev1 R324 and the incoming dATP (conformation 1). Hydrogen bonds are shown as black dashed lines and hydrogen bonding distances (\AA) are labeled. **c** Two focused views of the hydrogen bonds formed between Rev1 R324 and the incoming dATP (conformation 2). Hydrogen bonds are shown as black dashed lines and hydrogen bonding distances (\AA) are labeled. **d** An overlay of the Rev1/DNA/dATP ternary complex (conformation 1, pink sticks) and Rev1/DNA/dCTP ternary complex (gray sticks) showing differences in the position of the primer terminal dG 3'-OH. Red arrows and the respective distances (\AA) show the movement of the primer terminal dG 3'-OH between the two structures. **e** An overlay of the Rev1/DNA/dATP ternary complex (conformation 2, pink sticks) and Rev1/DNA/dCTP ternary complex (gray sticks) showing differences in the position of the primer terminal dG 3'-OH. Red arrows and the respective distances (\AA) show the movement of the primer terminal dG 3'-OH between the two structures.

To understand how Rev1 interacts with incoming dATP, we determined a 1.8 \AA structure of the Rev1/DNA/dATP ternary complex (Supplementary Table 2). The overall structure of the Rev1-dATP ternary complex is very similar to the Rev1-dCTP ternary complex, including the evicted templating guanine base, the R324 protein template, and the important Rev1 active site side chains (RMSD = 0.331, Supplementary Fig. 3). However, major alterations to the conformation of the dATP and the primer terminal dG base were observed (Fig. 4 and Supplementary Fig. 3). Figure 4a shows a close-up of the Rev1-dATP ternary complex active site, which contains the incoming dATP and both Ca_n and Ca_c ions. Interestingly, we observed two dATP conformations in the Rev1 active site. In both conformations, the dATP base adopts the Hoogsteen conformation, with the Hoogsteen edge facing the R324 protein-template. In conformation 1, the dATP forms a single non-planar hydrogen bond between the N7 of the Hoogsteen edge and the Ne of R324

(Fig. 4b). In conformation 2, the dATP forms a single non-planar hydrogen bond between the N7 of the dATP Hoogsteen edge and the Ne of R324, but the incoming dATP has undergone a 1.7 \AA downward movement in relation to R324 that was not seen in dATP conformation 1 (Fig. 4c). Additional differences in the conformation of the dATP ribose sugar were observed. In the dATP conformation 1, the ribose sugar adopts a $C4'$ -exo sugar pucker. (Fig. 4d). In the dATP conformation 2, the ribose sugar adopts a $C2'$ -endo sugar pucker (Fig. 4e). Notably, the sugar puckers for both dATP conformations are different than the $C3'$ -endo sugar pucker observed for incoming dCTP. Structural superimposition of the Rev1-dATP and Rev1-dCTP ternary complex structures identified additional changes within the active site with implications for catalysis (Fig. 4d, e). The non-planar interactions of both dATP conformation 1 and 2 leads to a 1.1 \AA movement of the primer terminal dG 5'-phosphate, which results in a 1.0 \AA movement of the 3'-OH distal to the Pa of the

incoming dATP. This brings the 3'-OH to 4.0 Å and 4.4 Å from Pa of the dATP in conformation 1 and 2, respectively (Fig. 4d, e). In both conformations, the 3'-OH is not in the proper conformation for in-line nucleophilic attack on Pa of the incoming dATP. Together, this indicates that the Hoogsteen conformation of the dATP leads to the reduction in nucleotide binding, while the movement in the 3'-OH distal to the Pa explains the decrease in catalysis that was previously described for Rev1 insertion of dATP (Supplementary Table 1)^{36,37}.

Dynamics of the Rev1-dNTP ternary complex active sites. Our structural analysis indicates that Rev1 binds incoming dTTP, dGTP, and dATP through sub-optimal hydrogen bonds with R324. However, these structures represent static snapshots of the interaction between R324 and the incoming nucleotide in the Rev1 active site. To further understand the stability and dynamics of the R324 interaction with different incoming dNTPs, we performed duplicate 1 μs MD simulations on the Rev1-dTTP, Rev1-dGTP, and Rev1-dATP ternary complex structures and compared them to previous MD simulations of the Rev1-dCTP ternary complex³⁴. Notably, we observed stable hydrogen bonds between the Ne and Nη of R324 and the O2 and N3 of the dCTP during the previous Rev1-dCTP ternary complex simulation (Supplementary Fig. 4)³⁴. In contrast, sub-optimal hydrogen bonding was observed for R324 with dTTP, dGTP, and dATP throughout the MD simulations (Fig. 5 and Supplementary Fig. 5). In the Rev1-dTTP ternary complex MD simulations, a single hydrogen bond was observed between the Ne of R324 and the O2 of dTTP, but only during 26.1 ± 9.1% of trajectories (Fig. 5a and Supplementary Fig. 5a). This single hydrogen bond is consistent with the Rev1-dTTP ternary complex crystal structure but suggests the R324 interaction with dTTP is dynamic (Fig. 2b). In the Rev1-dGTP ternary complex MD simulations, two hydrogen bonds were observed between the Ne and Nη of the R324 the N7 and O6 of the dGTP Hoogsteen edge during 81.9 ± 12.2% and 86.8 ± 10.7% of the MD simulation, respectively (Fig. 5b and Supplementary Fig. 5b). These two hydrogen bonds are consistent with the Rev1-dGTP ternary complex crystal structure (Fig. 3b), but indicates the dGTP undergoes moderate dynamic fluctuations when interacting with R324. Finally, we observed minimal interaction between R324 with dATP during the MD simulations, with a single hydrogen bond observed between the Ne of R324 and the N7 of dATP Hoogsteen edge during only 7.1 ± 3.7% of the MD simulation (Fig. 5c and Supplementary Fig. 5c). The minimal interaction of R324 and dATP during the simulation suggests the dATP base is highly dynamic, consistent with the multiple conformations observed in the Rev1-dATP ternary complex crystal structure (Fig. 4b, c). Together, these simulations indicate the interactions of R324 with dTTP, dGTP, and dATP are less stable than dCTP (compare Fig. 5 and Supplementary Fig. 4). The sub-optimal hydrogen bonds and less stable interaction with R324 explains the reduction in nucleotide binding previously described for Rev1-mediated insertion of dTTP, dGTP, and dATP (Supplementary Table 1)^{36,37}.

During both Rev1-dATP ternary complex simulations, we also observed a significant conformational change in the dATP base that corresponds to a switch from the Hoogsteen conformation to the Watson-Crick conformation (Fig. 5c and Supplementary Fig. 5c). The dATP Watson-Crick face has a single hydrogen bond acceptor (dATP N1) that could potentially interact with the Ne or Nη of R324. However, we did not observe an interaction between the Ne or Nη of R324 and the N1 of the dATP Watson-Crick edge during the time the dATP adopted the Watson-Crick conformation during these trajectories, nor during additional MD simulations starting with the dATP in a Watson-Crick

conformation (Supplementary Fig. 6). Notably, dATP has the largest reduction in catalytic efficiency for Rev1-mediated insertion (Supplementary Table 1)^{36,37}, and the significant conformational changes during the Rev1-dATP ternary complex MD simulations provide a further rationale for this finding.

Structural basis for Rev1 sugar selectivity. In addition to DNA base discrimination, DNA polymerases must also maintain sugar selectivity to preferentially incorporate dNTPs rather than rNTPs. This is generally accomplished through a steric gate and/or polar filter residue that prevents ribonucleotide binding and incorporation. Despite the presence of both a steric gate and polar filter residue, Rev1 displays poor sugar selectivity inserting dCTP with a relative catalytic efficiency that is 280-fold higher than rCTP (Supplementary Table 1)³⁷. Notably, this sugar selectivity is orders of magnitude worse than most DNA polymerases^{11,12}. To obtain mechanistic insight into the sugar selectivity by Rev1, we determined a 1.75 Å structure of the Rev1/DNA/rCTP ternary complex (Supplementary Table 2).

The overall Rev1-rCTP ternary complex structure is very similar to the Rev1-dCTP ternary complex structure (RMSD = 0.258 Å), including the evicted templating guanine base, the R324 protein template, and important Rev1 active site side chains (Supplementary Fig. 7a). However, we observed significant differences in the conformation of the incoming rCTP sugar and the primer terminal dG base (Fig. 6 and Supplementary Fig. 7a). Figure 6a shows a close-up of the active site for the Rev1-rCTP ternary complex, which contains the incoming rCTP and both Ca_n and Ca_c ions. The rCTP base forms two planar hydrogen bonds with the R324 protein template utilizing the N2 and O6 of the Watson-Crick face and the Ne and Nη of the R324 guanidinium group (Fig. 6b). This interaction of the rCTP with R324 is very similar to the interaction of the incoming dCTP and R324 (Fig. 1a and Supplementary Fig. 7a). Notably, a significant conformational change was observed in the ribose sugar of the rCTP, which adopts a C2'-endo sugar pucker compared to the C3'-endo sugar pucker observed for incoming dCTP (Fig. 6c and Supplementary Fig. 7b). In this conformation, the closest distance between the 2'-OH and F367 is 3.2 Å, indicating the 2'-OH does not significantly clash with the Rev1 F367 steric gate (Fig. 6c). In contrast, if the rCTP was in a C3'-endo sugar pucker the 2'-OH would significantly clash with the F367 steric gate (Fig. 6c). Rev1 also possesses a polar filter residue (S402), which is thought to interact with the 3'-OH of the incoming nucleotide and position the C2' in close proximity to the steric gate (Supplementary Fig. 7c)¹³. This interaction would provide an additional layer of discrimination for dCTP over rCTP. Interestingly, the C2'-endo sugar pucker leads to a conformation of the rCTP 3'-OH that does not interact with the S402 polar filter residue (Supplementary Fig. 7c). Taken together, the C2'-endo sugar pucker of the rCTP prevents significant clashing with Rev1, thus enabling the active site to readily accommodate insertion of ribonucleotides.

The change in the rCTP sugar pucker prevents the 2'-OH from clashing with the Rev1 steric gate. However, comparison of the Rev1-rCTP and Rev1-dCTP ternary complex structures revealed several additional conformational changes in the Rev1 active site that likely effect catalysis (Fig. 6d). The C2'-endo sugar pucker of the rCTP results in a 1.3 Å downward movement in the ribose sugar towards the primer terminal dG, which results in a 1.6 Å movement of the primer terminal dG away from the rCTP. In this conformation, the 3'-OH of the primer terminal dG is 5.4 Å away from the Pa of the rCTP and not in proper position for the in-line nucleophilic attack. Therefore, the Rev-rCTP ternary complex structure provides a rational for comparable dCTP and rCTP binding to Rev1, while also explaining the decrease in catalysis

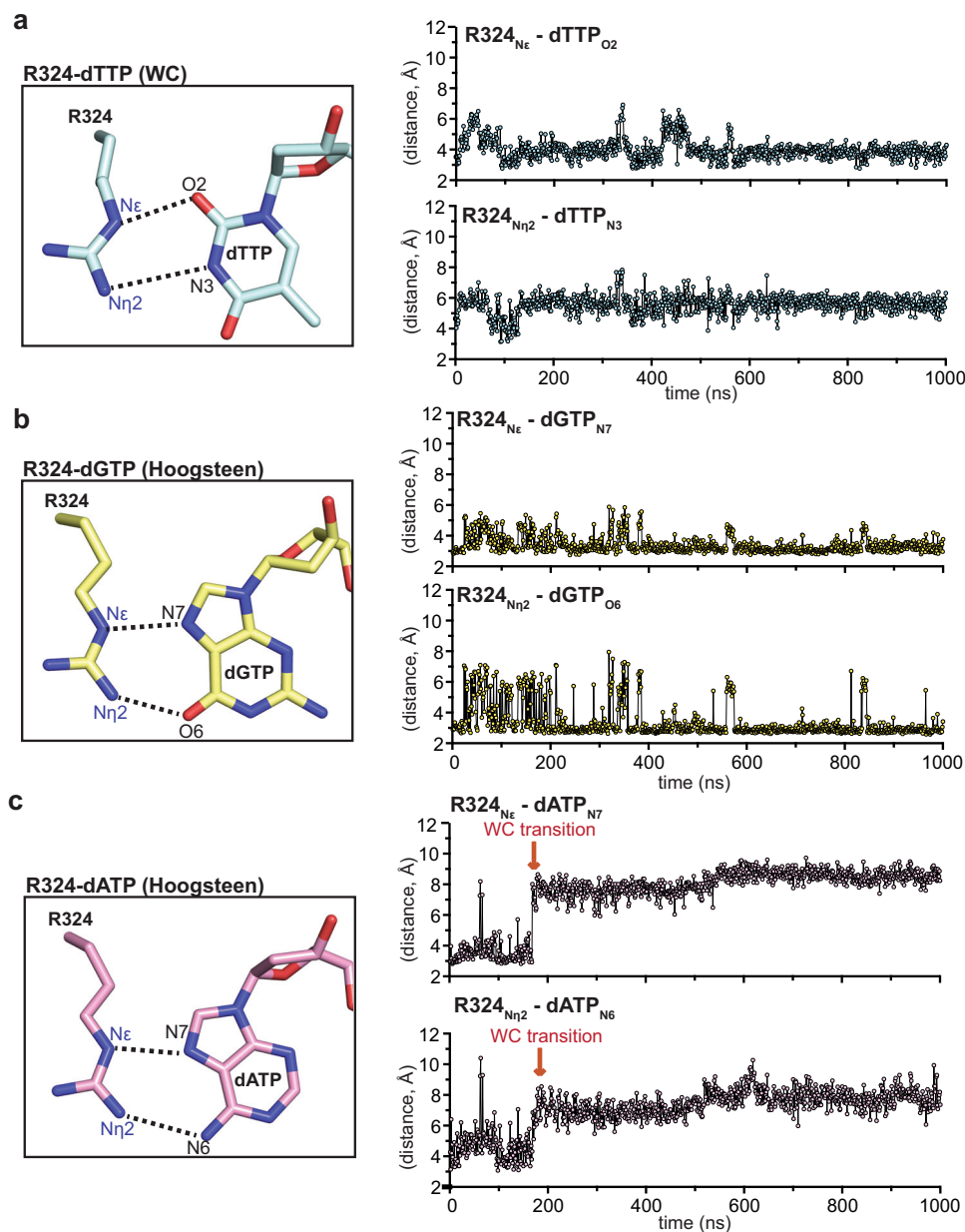


Fig. 5 Molecular dynamics simulations of the Rev1/DNA/dNTP ternary complex structures. **a** Focused view of the Rev1 R324 side chain and incoming dTTP (Watson-Crick conformation) showing the distances monitored throughout the MD simulation (left). Representative distance profiles for $R324_{Ne}$ -dTTP_{O2} and the $R324_{N\eta 2}$ -dTTP_{N3} in the Rev1/DNA/dTTP ternary complex simulation (right). Each datapoint represents the distance (Å) between the indicated atoms at a single snapshot (1 ns) from the MD simulation. The replicate experiment can be found in Supplementary Fig. 5a. **b** Focused view of the Rev1 R324 side chain and incoming dGTP (Hoogsteen conformation) showing the distances monitored throughout the MD simulation (left). Representative distance profiles for $R324_{Ne}$ -dGTP_{N7} and the $R324_{N\eta 2}$ -dGTP_{O6} in the Rev1/DNA/dGTP ternary complex simulation (right). Each datapoint represents the distance (Å) between the indicated atoms at a single snapshot (1 ns) from the MD simulation. The replicate experiment can be found in Supplementary Fig. 5b. **c** Focused view of the Rev1 R324 side chain and incoming dATP (Hoogsteen conformation) showing the distances monitored throughout the MD simulation (left). Representative distance profiles for $R324_{Ne}$ -dATP_{N7} and the $R324_{N\eta 2}$ -dATP_{N6} in the Rev1/DNA/dATP ternary complex simulation (right). Each datapoint represents the distance (Å) between the indicated atoms at a single snapshot (1 ns) from the MD simulation. The dATP transition from Hoogsteen to Watson-Crick conformation is denoted with a red arrow. The replicate experiment can be found in Supplementary Fig. 5c. Source data for this figure are provided as a Source Data file.

during Rev1-mediated insertion of rCTP through alterations in the primer terminal 3'-OH³⁷.

Dynamics of the Rev1-rCTP ternary complex active site. Our structural analysis indicates that the incoming rCTP adopts a C2'-endo ribose sugar pucker, which enables the formation of stable

hydrogen bonds between the rCTP and R324 in the Rev1 active site. To obtain additional insight into the stability and dynamics of the R324-rCTP interaction and the rCTP sugar pucker, we performed duplicate 1 μs MD simulations on the Rev1-rCTP ternary complex structure. During the Rev1-rCTP ternary complex simulation, the O2 and N3 of the rCTP Watson-Crick edge and the Ne and Nη were observed within hydrogen bonding

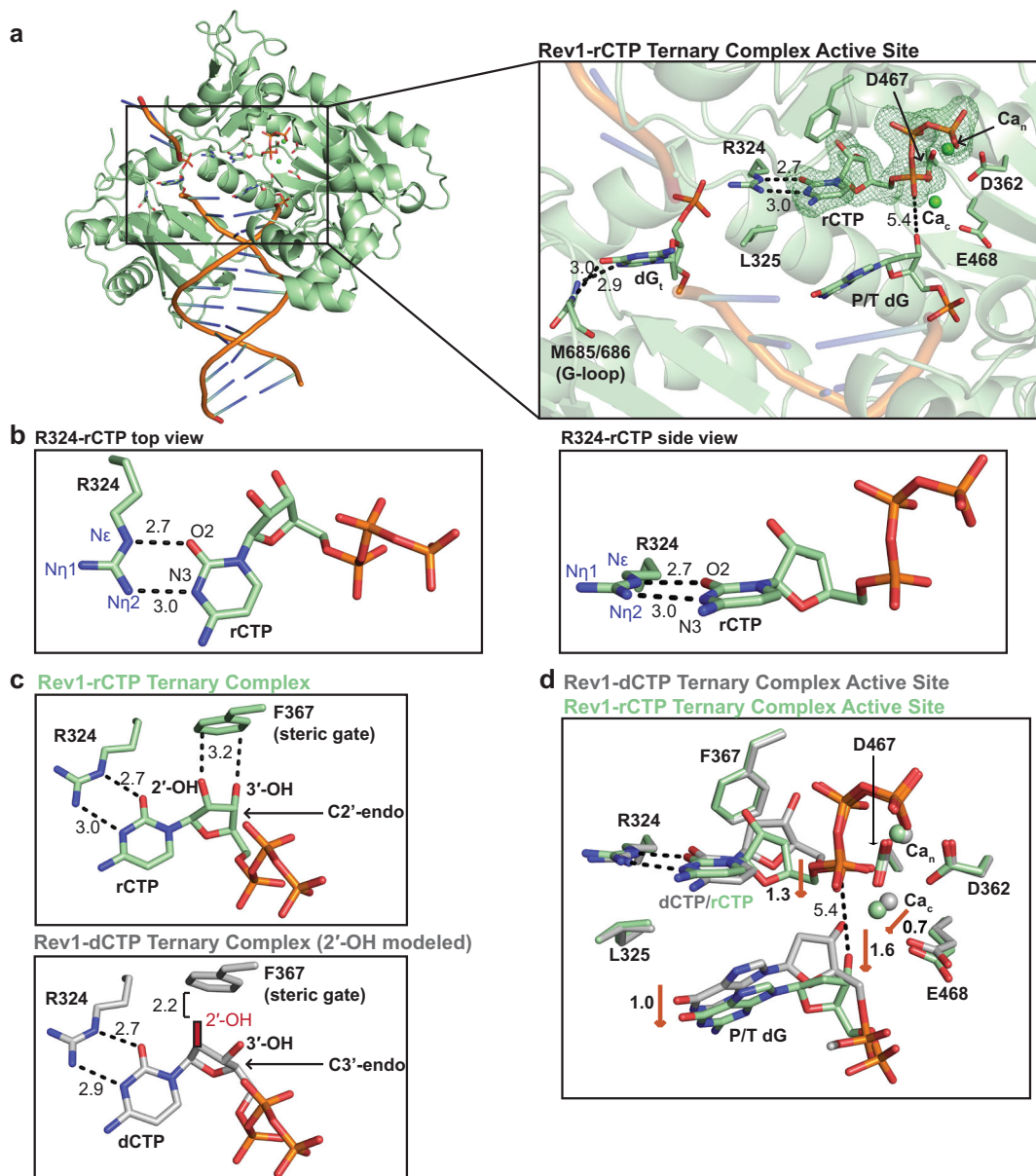


Fig. 6 Rev1/DNA/rCTP ternary complex structure. **a** An overall structure (left) and active site closeup (right) of the Rev1/DNA/rCTP ternary complex. Key protein and DNA residues are shown as green sticks. The nucleotide binding (Ca_n) and catalytic (Ca_c) metals are shown as green spheres. A Polder OMIT map contoured at $\sigma = 3.0$ for the incoming rCTP is shown as a green mesh. **b** Two focused views of the hydrogen bonds formed between Rev1 R324 and the incoming rCTP. Hydrogen bonds are shown as black dashed lines and hydrogen bonding distances (Å) are labeled. **c** A focused view of the incoming nucleotide position in comparison to the Rev1 F367 steric gate residue in the Rev1/DNA/rCTP (green sticks, top) and Rev1/DNA/dCTP (gray sticks, bottom) ternary complex structures. Key distances (Å) are shown as black dashed lines. The 2'-OH in the Rev1/DNA/dCTP complex is modeled. **d** An overlay of the Rev1/DNA/rCTP ternary complex (green sticks) and Rev1/DNA/dCTP ternary complex (gray sticks). Red arrows and the respective distances (Å) highlight key active site differences between the two structures. The nucleotide binding (Ca_n) and catalytic (Ca_c) metals are shown as spheres.

distance for 100% and 99.9% of the MD trajectory, respectively (Fig. 7a and Supplementary Fig. 8a). This indicates the rCTP forms a stable interaction with R324, similar to the Rev1-dCTP ternary complex structure (Supplementary Fig. 4). To understand the stability and dynamics of the rCTP sugar pucker, we monitored the pseudorotation angle of the rCTP ribose sugar throughout the MD simulation, which reports on the sugar pucker of the rCTP ribose. The average pseudorotation angle of the rCTP sugar was 186.3 ± 0.4 throughout the simulation, indicating the rCTP largely adopts a C2'-endo sugar pucker in the Rev1 active site (Fig. 7b and Supplementary Fig. 8b). Importantly, this highlights the stability of the C2'-endo sugar pucker observed

in the Rev1-rCTP ternary complex crystal structure (Fig. 6b). In contrast to rCTP, the dCTP ribose largely adopts a C3'-endo sugar pucker throughout the simulation, though moderate sampling of the C2'-endo sugar pucker was observed (Fig. 7c). The stability of the C2'-endo sugar pucker and hydrogen bonds between R324 and the rCTP base likely explain the comparable affinity of Rev1 for rCTP and dCTP^{36,37}.

Discussion

Rev1 utilizes a protein-template mechanism for DNA base discrimination, where the side chain of R324 forms two stabilizing

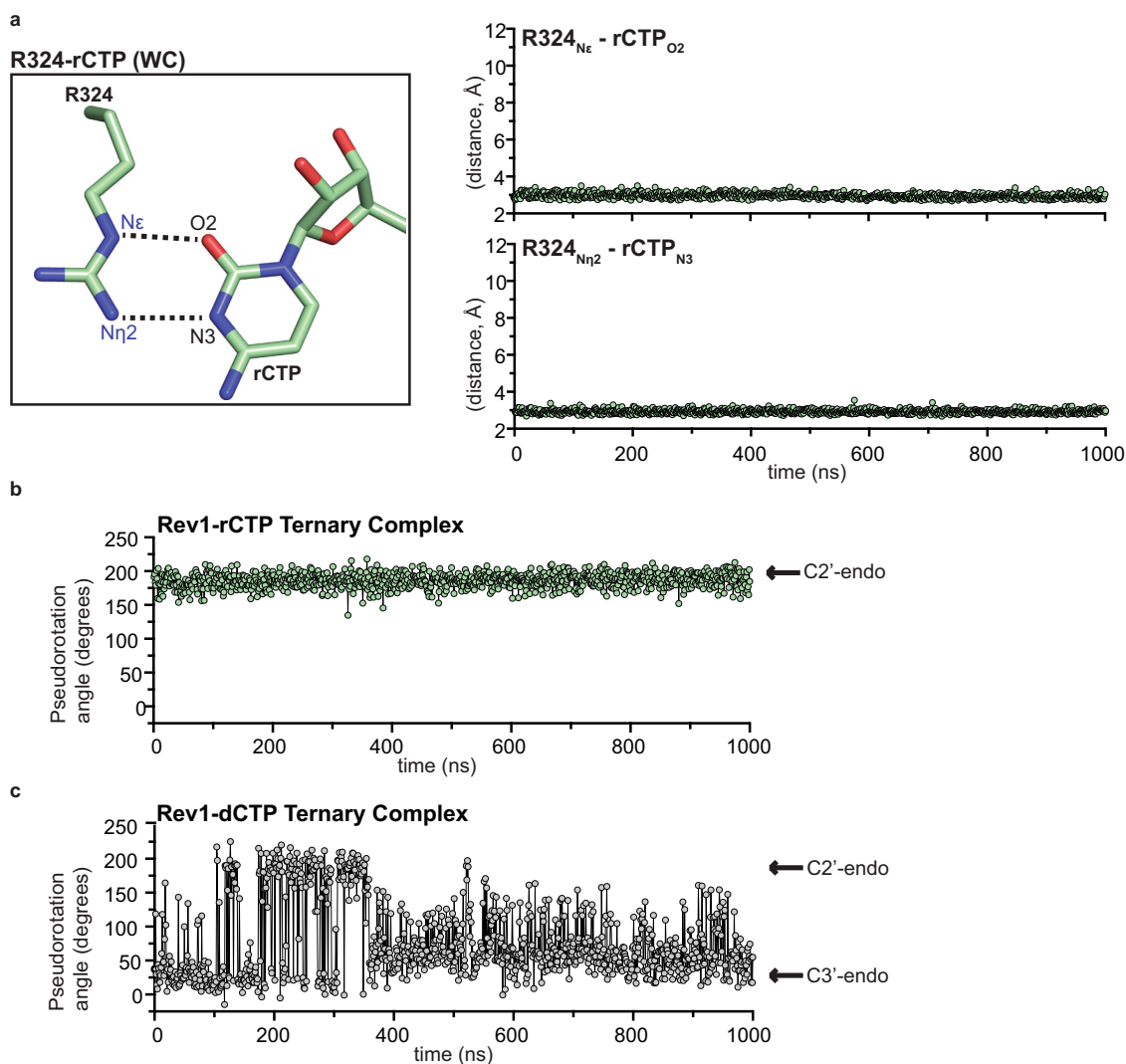


Fig. 7 Molecular dynamics simulation of the Rev1/DNA/rCTP ternary complex structure. **a** Focused view of the Rev1 R324 side chain and incoming rCTP (Watson-Crick conformation) showing the distances monitored throughout the MD simulation (left). Representative distance profiles for R324_{Ne}-rCTP_{O2} and the R324_{Nn2}-rCTP_{N3} in the Rev1/DNA/rCTP ternary complex MD simulation (right). Each datapoint represents the distance (Å) between the indicated atoms at a single snapshot (1 ns) from the MD simulation. The replicate experiment can be found in Supplementary Fig. 8a. **b** Representative pseudorotation angle profile for the rCTP ribose sugar throughout the MD simulation. Each datapoint represents the pseudorotation angle of the rCTP ribose sugar at a single snapshot (1 ns) from the MD simulation. The replicate experiment can be found in Supplementary Fig. 8b. **c** Pseudorotation angle profiles for the dCTP ribose sugar throughout the MD simulation³⁴. Each datapoint represents the pseudorotation angle of the dCTP ribose sugar at a single snapshot (1 ns) from the MD simulation. Source data for this figure are provided as a Source Data file.

hydrogen bonds with the incoming dCTP (Fig. 1). Notably, similar stabilizing hydrogen bonds are unable to be formed with incoming dTTP, dGTP, or dATP, which has led to the hypothesis that R324 may act as a gate to prevent binding of mismatched incoming nucleotides. Notably, this hypothesis has proven difficult to address in the absence of high-resolution structures of Rev1 in complex with mismatched incoming dNTPs. Our work has provided novel mechanistic insight into how Rev1 utilizes the R324 protein template to prevent optimal hydrogen bonding with incoming dTTP, dGTP, and dATP, thus accounting for the enzyme's substrate specificity. The Rev1-dTTP ternary complex structure indicates that incoming dTTP binding is accomplished through a single non-planar hydrogen bond with R324, which is different than the two hydrogen bonds seen for incoming dCTP (Fig. 2). The non-planar interaction of dTTP and R324 results in a conformation of the 3'-OH of the primer terminal nucleotide that is not in proper orientation for catalysis. These structural

changes explain the ~10-fold decrease in dissociation constant (K_d) for dTTP binding and ~26-fold decrease in nucleotide incorporation (k_{pol}) previously determined for Rev1 insertion of dTTP using pre-steady state kinetics methods³⁷. Next, the Rev1-dGTP ternary complex structure shows that incoming dGTP adopts a Hoogsteen conformation, which allows the dGTP to form two non-planar hydrogen bonds with R324 (Fig. 3). In this conformation, the dGTP is readily accommodated in the spacious Rev1 active site, and results in minimal changes to the 3'-OH of the primer terminal nucleotide. The structural changes to dGTP and minimal changes to the primer terminal 3'-OH are consistent with the ~45-fold decrease in dissociation constant for dGTP binding and a modest ~3.5-fold decrease in nucleotide incorporation. Finally, the Rev1-dATP ternary complex structure indicates the dATP is dynamic adopting two distinct conformations in the Rev1 active site. In both conformations, the dATP is in the Hoogsteen conformation and forms a single non-planar

hydrogen bond with R324 (Fig. 4). The non-planar interactions lead to a conformation of the 3'-OH of the primer terminal nucleotide that is not in proper orientation for catalysis. These structural changes explain the ~30-fold decrease in dissociation constant for dATP binding and a ~450-fold decrease in nucleotide incorporation for Rev1 insertion of dATP.

Substantial evidence indicates that DNA polymerases select and incorporate the correct dNTP using an induced-fit mechanism, where the DNA polymerase undergoes conformational changes during dNTP binding and sampling of proper Watson-Crick base pairing with the templating DNA base^{4–8}. We previously showed Rev1 does not undergo a conformational change upon incoming nucleotide binding³⁴, nor does Rev1 use a templating DNA base for coordination of the incoming nucleotide during the catalytic cycle^{29–31,33}. The Rev1 ternary complex structures described here highlight how fidelity is maintained through sub-optimal hydrogen bonds of dTTP, dGTP, and dATP with the R324 protein-templating. Importantly, this is analogous to the sub-optimal hydrogen bonds between mismatched dNTPs and templating DNA bases for other DNA polymerases. We also identified conformational changes to the primer terminal DNA base that result in a Rev1 active site where the 3'-OH is not in position for the in-line nucleophilic attack on the Pa of the incoming dNTP. This is consistent with the other DNA polymerases, where the 3'-OH is not properly aligned with Pa of the incoming dNTP during insertion of mismatched nucleotides^{9,10,38–40}. Consistently, our MD simulations show that dTTP, dGTP, and dATP form dynamic and sub-optimal hydrogen bonds with R324 in the Rev1 active site. Together, this suggests that optimal hydrogen bonding with the incoming nucleotide and stringent active site organization of the primer terminal 3'-OH are mis-insertion checkpoints used by all DNA polymerases, irrespective of whether a templating DNA base is utilized.

In addition to DNA base discrimination, DNA polymerases must also choose the incoming nucleotide with the correct sugar. This is particularly challenging given that the cellular concentration of ribonucleotides are in vast excess of deoxyribonucleotides^{41,42}. For most DNA polymerases, ribonucleotide discrimination is accomplished through a bulky aromatic steric gate residue, which prevents efficient binding of rNTPs via steric clashes with the 2'-OH^{11,12}. In some cases, the steric gate can also be supplemented with a polar filter, which interacts with the 3'-OH and brings the C2' in close proximity to the steric gate¹³. Interestingly, as shown by pre-steady state kinetics, hRev1 binds rCTP with a similar K_d as dCTP, but has a 280-fold decrease in catalysis, indicating that Rev1 sugar discrimination occurs at the catalytic step and not nucleotide binding. The modest sugar fidelity of Rev1 has been perplexing, as Rev1 possesses both a steric gate (F367) and polar filter (S210) residue. Our Rev1-rCTP ternary complex structure and MD simulations provide a rationale for this observation. In the Rev1 active site, the rCTP adopts a C2'-endo sugar pucker that prevents significant clashes with the F367 steric gate (Fig. 6). In addition, the conformation observed for the rCTP is incapable of forming an interaction with the S210 polar filter. This indicates the C2'-endo sugar pucker prevents the incoming rCTP from clashing with the steric gate and polar filter active site residues, and ultimately explains the similar affinity of Rev1 for incoming rCTP and dCTP. Although Rev1 interacts with rCTP and dCTP with similar affinity, a decrease in catalysis for rCTP has been observed³⁷. Our structures indicate the decrease in catalysis during Rev1 insertion of rCTP is due to a conformational change in the 3'-OH of the primer terminal DNA base, which arises from the rCTP adopting a 2'-endo sugar pucker in the Rev1 active site. This prevents proper Rev1 active site organization for phosphodiester bond formation between the 3'-OH and the Pa of the incoming nucleotide, which is similar to observations for DNA Pol β and Pol η

during mis-insertion of ribonucleotides^{43,44}. Notably, the mechanism for ribonucleotide discrimination by Rev1 is different than that observed for Pol μ and Pol λ^{45,46}, underscoring the importance of studying mechanisms of ribonucleotide discrimination for different DNA polymerases.

Our structural studies have provided novel insight into how the R324 protein-templating enables Rev1 to maintain preferential insertion of dCTP. Importantly, the preferential insertion of dCTP by Rev1 is advantageous during multiple cellular processes. For example, Rev1 accommodates several forms of adducted guanine bases in its active site, which is important for DNA damage bypass during TLS^{30,31,33}. In addition, Rev1 is known to perform DNA synthesis across from G-quadruplex sequences during DNA replication^{15,16,47}. In these biological contexts, it is critical for Rev1 to maintain preferential insertion of dCTP to ensure maintenance of the DNA coding potential. More recently, Rev1 has also been implicated in replication-induced gap filling, which may be a vulnerability in cancer cells^{17,48}. Consistently, inhibition of Rev1 function has shown promise as a chemotherapeutic adjuvant^{49–51}, underscoring the importance for further characterizing the molecular basis of Rev1 function.

The cellular concentrations of rCTP are in vast excess of dCTP⁴¹. Given the modest sugar fidelity of Rev1 in vitro, dCTP and rCTP are likely inserted at similar efficiencies during TLS in vivo³⁷. Interestingly, the TLS polymerases Pol η and Pol ι also maintain modest sugar selectivity compared to replicative DNA polymerases in vitro^{52,53}. The poor sugar fidelity by TLS polymerases suggests that DNA damage bypass during replication may contribute a small proportion of ribonucleotides found embedded in the genome. Interestingly, RNase H2 is the enzyme responsible for processing ribonucleotides embedded in DNA, and is known to interact with the core TLS component PCNA at stalled replication forks^{54–57}. The interaction of PCNA and RNase H2 may allow for the rapid removal of mis-inserted ribonucleotides after DNA damage bypass by the ribonucleotide excision repair (RER) pathway⁴². However, recent evidence suggests that RNase H2 activity is decreased when removing ribonucleotides across from DNA damage⁵², indicating that removal of ribonucleotides after DNA damage bypass by TLS polymerases may be inefficient. It is interesting to speculate whether TLS polymerases may contribute to the accumulation of ribonucleotides in the genome, though additional work is needed to understand the complex interplay between ribonucleotide mis-incorporation during TLS and RNase H2-dependent RER pathways.

Methods

Preparation of DNA substrates. For X-ray crystallography, oligonucleotides 5'-ATC-GCT-ACC-ACA-CCC-CT-3' (template strand) and 5'-GGG-GTG-TGG-TAG-3' (primer strand) were resuspended in a buffer containing 10 mM Tris-8.0 and 1 mM EDTA and annealed by heating to 90 °C for 5 min before cooling to 4 °C using a linear gradient (−1 °C min^{−1}).

Expression and purification of Rev1. The construct for the *Saccharomyces cerevisiae* (yeast) Rev1 catalytic core was purchased from GenScript. All Rev1 constructs were transformed and expressed in BL21(DE3) plyS E. coli cells (Invitrogen). Cells were grown at 37 °C until an OD₆₀₀ ~0.7 was reached. Rev1 protein expression was induced with 0.1 mM IPTG at 20 °C overnight. The resulting cell pellets were frozen and stored at −20 °C, or −80 °C for longer term storage. For cell lysis, Rev1 cell pellets were resuspended in a lysis buffer containing 50 mM HEPES (pH-7.4), 150 mM NaCl, 1 mM EDTA, 1 mM DTT and a cocktail of protease inhibitors. The cells were lysed via sonication and the lysate cleared at 24,000 xg for one hour. The supernatant containing GST-Rev1 protein was incubated with glutathione agarose resin (Goldbio) for 2 hours, washed on the glutathione resin with a high salt buffer containing 50 mM HEPES and 1 M NaCl, and the GST-tag cleaved off overnight using PreScission Protease. The cleaved Rev1 protein was purified by cation-exchange chromatography using a POROS HS column (GE Health Sciences) and gel filtration using a HiPrep 16/60 Sephacryl S-200 HR (GE Health Sciences). The purified Rev1 protein was frozen and stored at −80 °C in a buffer containing 250 mM NaCl, 50 mM Tris (pH-8.0), and 2 mM TCEP.

X-ray crystallography. Oligonucleotides 5'-ATC-GCT-ACC-ACA-CCC-CT-3' (template strand) and 5'-GGG-GTG-TGG-TAG-3' (primer strand) were utilized for all X-ray crystallography experiments. The annealed DNA substrate (1.15 mM) was mixed with Rev1 protein (5–6 mg ml⁻¹) and the Rev1/DNA binary crystals obtained in a condition with the reservoir containing 15–23% PEG3350 and 200 mM ammonium nitrate using the sitting-drop vapor diffusion method. To generate the dTTP and rCTP ternary complex structures, the Rev1/DNA binary crystals were transferred to a cryoprotectant containing reservoir solution, 25% glycerol, 50 mM CaCl₂ and 10 mM of dTTP or rCTP. Attempts to soak in dATP and dGTP into the Rev1 active site were unsuccessful. To generate dATP and dGTP ternary complex structures, the Rev1 protein (5–6 mg ml⁻¹), annealed DNA substrate (1.15 mM), 50 mM CaCl₂, and dATP (1 mM) or dGTP (20 mM) were mixed and crystals obtained in a condition with the reservoir containing 15–23% PEG3350 and 200 mM ammonium nitrate using the sitting-drop vapor diffusion method. The dATP and dGTP ternary complex crystals were transferred to a cryoprotectant containing reservoir solution and 25% glycerol. All X-ray crystallography data were collected at 100 K on a Rigaku MicroMax-007 HF rotating anode diffractometer equipped with a Dectris Pilatus3R 200K-A detector system at a wavelength of 1.54 Å. Initial models were generated by molecular replacement using a previously solved Rev1/DNA/dCTP ternary complex (PDB: 6X6Z or 5WMI) as a reference structure. Further refinement and model building was carried out using PHENIX and Coot, respectively^{58,59}. All figures containing structures were generated using PyMOL (Schrödinger LLC)⁶⁰. The sugar puckers for incoming NTPs were determined by calculating pseudorotation angles using the web 3DNA server⁶¹.

MD simulations. Molecular dynamics (MD) simulations were performed for Rev1 and DNA complexes in explicit water solvent, using a protocol similar to our previous study³⁴. Model preparation and simulations were performed using the AMBER v16 suite of programs for biomolecular simulations⁶². AMBER's *ff14SB*⁶³ force-fields were used for all simulations. MD simulations were performed using NVIDIA graphical processing units (GPUs) and AMBER's *pmemd.cuda* simulation engine using our lab protocols published previously^{64,65}. We have verified the suitability of *ff14SB* for simulations at microsecond timescales for multiple proteins and protein-DNA complexes^{34,66,67}. Standard parameters from *ff14SB* force-field were used for the protein residues and nucleotides. Non-standard nucleotides (dATP dCTP, dGTP, dTTP, and rCTP) were parameterized using procedure described in the AMBER manual. The AMBER library file for these nucleotides is available in the supporting information. SPC model was used for water. The parameters for ions were used from AMBER, as available in the *frmod.ionsjc_spce* and *frmod.ionslrcm_hfe_spce* files.

A total of 10 separate simulations were performed for Rev1-dTTP, Rev1-dGTP, Rev1-dATP (in Hoogsteen conformation, conformation 2) Rev1-dATP (in Watson-Crick conformation) and Rev1-rCTP based on the Rev1-NTP ternary complex X-ray crystal structures determined in this study. These ten separate simulations represent duplicate experiments for each of the 5 Rev1-NTP ternary complex structures. The missing hydrogen atoms were added by AMBER's leap program. After processing the coordinates of the protein and substrate, all systems were neutralized by addition of counter-ions and the resulting system were solvated in a rectangular box of SPC/E water, with a 10 Å minimum distance between the protein and the edge of the periodic box. The prepared systems were equilibrated using a protocol described previously^{68,69}. The equilibrated systems were then used to run 1.0 μs of production MD under constant energy conditions (NVE ensemble). The use of NVE ensemble is preferred as it offers better computational stability and performance^{70,71}. The production simulations were performed at a temperature of 300 K. As NVE ensemble was used for production runs, these values correspond to initial temperature at start of simulations. Temperature adjusting thermostat was not used in simulations; over the course of 1.0 μs simulations the temperature fluctuated around 300 K with RMS fluctuations between 2–4 K, which is typical for well equilibrated systems. A total of 1000 conformational snapshots (stored every 1000 ps) collected for each system was used for analysis.

Distance profile calculations: The distances and percentage occupancy were calculated using the 1000 conformational snapshots stored during the MD simulations. A cutoff of 3.5 Å was used to calculate the percent of snapshots within hydrogen bonding distance (occupancy) during each MD simulation.

Reporting summary. Further information on research design is available in the Nature Research Reporting Summary linked to this article.

Data availability

The data that support this study are available from the corresponding authors upon reasonable request. Atomic coordinates and structure factors for the crystal structures reported in this manuscript have been deposited with the Protein Data bank under accession numbers 7T18, 7T19, 7T1A, and 7T1B. Atomic coordinates and structure factors for the previously determined Rev1-dCTP ternary complex structure were accessed from the Protein Data bank under accession number 6X6Z. All molecular dynamics simulation trajectories have been deposited in the Data Archiving and Networking Services (DANS) repository and are available at <https://doi.org/10.17026/dans-xaw-36b2>. Source data are provided with this paper.

Received: 1 December 2021; Accepted: 6 May 2022;

Published online: 24 May 2022

References

- Wu, S., Beard, W. A., Pedersen, L. G. & Wilson, S. H. Structural comparison of DNA polymerase architecture suggests a nucleotide gateway to the polymerase active site. *Chem. Rev.* **114**, 2759–2774 (2014).
- Hoitsma, N. M. et al. Structure and function relationships in mammalian DNA polymerases. *Cell. Mol. Life Sci.* **77**, 35–59 (2020).
- Delagoutte, E. DNA polymerases: mechanistic insight from biochemical and biophysical studies. *Front Biosci. (Landmark Ed.)* **17**, 509–544 (2012).
- Steitz, T. A. DNA polymerases: structural diversity and common mechanisms. *J. Biol. Chem.* **274**, 17395–17398 (1999).
- Beard, W. A. & Wilson, S. H. Structural insights into DNA polymerase β fidelity: hold tight if you want it right. *Chem. Biol.* **5**, R7–R13 (1998).
- Beard, W. A. & Wilson, S. H. Structural insights into the origins of DNA polymerase fidelity. *Structure* **11**, 489–496 (2003).
- Doublé, S., Sawaya, M. R. & Ellenberger, T. An open and closed case for all polymerases. *Structure* **7**, R31–R35 (1999).
- Johnson, K. A. Role of induced fit in enzyme specificity: a molecular forward/reverse switch. *J. Biol. Chem.* **283**, 26297–26301 (2008).
- Freudenthal, B. D., Beard, W. A., Shock, D. D. & Wilson, S. H. Observing a DNA polymerase choose right from wrong. *Cell* **154**, 157–168 (2013).
- Batra, V. K., Beard, W. A., Shock, D. D., Pedersen, L. C. & Wilson, S. H. Structures of DNA polymerase β with active-site mismatches suggest a transient abasic site intermediate during misincorporation. *Mol. Cell* **30**, 315–324 (2008).
- Brown, J. A. & Suo, Z. Unlocking the sugar “steric gate” of DNA polymerases. *Biochemistry* **50**, 1135–1142 (2011).
- Vaisman, A. & Woodgate, R. Ribonucleotide discrimination by translesion synthesis DNA polymerases. *Crit. Rev. Biochem. Mol. Biol.* **53**, 382–402 (2018).
- Johnson, M. K., Kottur, J. & Nair, D. T. A polar filter in DNA polymerases prevents ribonucleotide incorporation. *Nucleic Acids Res.* **47**, 10693–10705 (2019).
- Sarkies, P., Reams, C., Simpson, L. J. & Sale, J. E. Epigenetic instability due to defective replication of structured DNA. *Mol. Cell* **40**, 703–713 (2010).
- Schiavone, D. et al. Determinants of G quadruplex-induced epigenetic instability in REV1-deficient cells. *EMBO J.* **33**, 2507–2520 (2014).
- Eddy, S. et al. Human Rev1 polymerase disrupts G-quadruplex DNA. *Nucleic Acids Res.* **42**, 3272–3285 (2014).
- Tagliatala, A. et al. REV1-Polζ maintains the viability of homologous recombination-deficient cancer cells through mutagenic repair of PRIMPOL-dependent ssDNA gaps. *Mol. Cell* **81**, 4008–4025.e7 (2021).
- Jansen, J. G. et al. Strand-biased defect in C/G transversions in hypermutating immunoglobulin genes in Rev1-deficient mice. *J. Exp. Med.* **203**, 319–323 (2006).
- Guo, C. et al. REV1 protein interacts with PCNA: significance of the REV1 BRCT domain in vitro and in vivo. *Mol. Cell* **23**, 265–271 (2006).
- Ohashi, E. et al. Interaction of hREV1 with three human Y-family DNA polymerases. *Genes Cells* **9**, 523–531 (2004).
- Johnson, R. E., Washington, M. T., Haracska, L., Prakash, S. & Prakash, L. Eukaryotic polymerases ι and ζ act sequentially to bypass DNA lesions. *Nature* **406**, 1015–1019 (2000).
- Powers, K. T. & Washington, M. T. Eukaryotic translesion synthesis: choosing the right tool for the job. *DNA Repair* **71**, 127–134 (2018).
- Boehm, E. M., Spies, M. & Washington, M. T. PCNA tool belts and polymerase bridges form during translesion synthesis. *Nucleic Acids Res.* **44**, 8250–8260 (2016).
- Nelson, J. R., Lawrence, C. W. & Hinkle, D. C. Deoxycytidyl transferase activity of yeast REV1 protein. *Nature* **382**, 729–731 (1996).
- Zhang, Y. et al. Response of human REV1 to different DNA damage: preferential dCMP insertion opposite the lesion. *Nucleic Acids Res.* **30**, 1630–1638 (2002).
- Haracska, L., Prakash, S. & Prakash, L. Yeast Rev1 protein is a G template-specific DNA polymerase. *J. Biol. Chem.* **277**, 15546–15551 (2002).
- Masuda, Y. & Kamiya, K. Biochemical properties of the human REV1 protein. *FEBS Lett.* **520**, 88–92 (2002).
- Masuda, Y., Takahashi, M., Fukuda, S., Sumii, M. & Kamiya, K. Mechanisms of dCMP transferase reactions catalyzed by mouse Rev1 protein. *J. Biol. Chem.* **277**, 3040–3046 (2002).
- Nair, D. T., Johnson, R. E., Prakash, L., Prakash, S. & Aggarwal, A. K. Rev1 employs a novel mechanism of DNA synthesis using a protein template. *Science* **309**, 2219–2222 (2005).
- Nair, D. T., Johnson, R. E., Prakash, L., Prakash, S. & Aggarwal, A. K. Protein-template-directed synthesis across an acrolein-derived DNA adduct by yeast Rev1 DNA polymerase. *Structure* **16**, 239–245 (2008).

31. Nair, D. T., Johnson, R. E., Prakash, L., Prakash, S. & Aggarwal, A. K. DNA synthesis across an abasic lesion by yeast REV1 DNA polymerase. *J. Mol. Biol.* **406**, 18–28 (2011).
32. Swan, M. K., Johnson, R. E., Prakash, L., Prakash, S. & Aggarwal, A. K. Structure of the human Rev1-DNA-dNTP ternary complex. *J. Mol. Biol.* **390**, 699–709 (2009).
33. Rechkoblit, O., Kolbanovskiy, A., Landes, H., Geacintov, N. E. & Aggarwal, A. K. Mechanism of error-free replication across benzo[a]pyrene stereoisomers by Rev1 DNA polymerase. *Nat. Commun.* **8**, 965 (2017).
34. Weaver, T. M. et al. Visualizing Rev1 catalyze protein-template DNA synthesis. *Proc. Natl Acad. Sci. USA* **117**, 25494–25504 (2020).
35. Howell, C. A., Prakash, S. & Washington, M. T. Pre-steady-state kinetic studies of protein-template-directed nucleotide incorporation by the yeast Rev1 protein. *Biochemistry* **46**, 13451–13459 (2007).
36. Pryor, J. M. & Washington, M. T. Pre-steady state kinetic studies show that an abasic site is a cognate lesion for the yeast Rev1 protein. *DNA Repair* **10**, 1138–1144 (2011).
37. Brown, J. A., Fowler, J. D. & Suo, Z. Kinetic basis of nucleotide selection employed by a protein template-dependent DNA polymerase. *Biochemistry* **49**, 5504–5510 (2010).
38. Arora, K., Beard, W. A., Wilson, S. H. & Schlick, T. Mismatch-induced conformational distortions in polymerase β support an induced-fit mechanism for fidelity. *Biochemistry* **44**, 13328–13341 (2005).
39. Krahn, J. M., Beard, W. A. & Wilson, S. H. Structural insights into DNA polymerase β deterrents for misincorporation support an induced-fit mechanism for fidelity. *Structure* **12**, 1823–1832 (2004).
40. Johnson, S. J. & Beese, L. S. Structures of mismatch replication errors observed in a DNA polymerase. *Cell* **116**, 803–816 (2004).
41. Traut, T. W. Physiological concentrations of purines and pyrimidines. *Mol. Cell. Biochem.* **140**, 1–22 (1994).
42. McElhinny, S. A. N. et al. Abundant ribonucleotide incorporation into DNA by yeast replicative polymerases. *Proc. Natl Acad. Sci.* **107**, 4949–4954 (2010).
43. Su, Y., Egli, M. & Guengerich, F. P. Mechanism of ribonucleotide incorporation by human DNA polymerase η . *J. Biol. Chem.* **291**, 3747–3756 (2016).
44. Cavanaugh, N. A. et al. Molecular insights into DNA polymerase deterrents for ribonucleotide insertion* \diamond . *J. Biol. Chem.* **286**, 31650–31660 (2011).
45. Moon, A. F. et al. Structural accommodation of ribonucleotide incorporation by the DNA repair enzyme polymerase μ . *Nucleic Acids Res.* **45**, 9138–9148 (2017).
46. Gosavi, R. A., Moon, A. F., Kunkel, T. A., Pedersen, L. C. & Bebenek, K. The catalytic cycle for ribonucleotide incorporation by human DNA Pol λ . *Nucleic Acids Res.* **40**, 7518–7527 (2012).
47. Ketkar, A. et al. Human Rev1 relies on insert-2 to promote selective binding and accurate replication of stabilized G-quadruplex motifs. *Nucleic Acids Res.* **49**, 2065–2084 (2021).
48. Nayak, S. et al. Inhibition of the translesion synthesis polymerase REV1 exploits replication gaps as a cancer vulnerability. *Sci. Adv.* **6**, eaaz7808 (2020).
49. Chatterjee, N. et al. REV1 inhibitor JH-RE-06 enhances tumor cell response to chemotherapy by triggering senescence hallmarks. *Proc. Natl Acad. Sci.* **117**, 28918–28921 (2020).
50. Wojtaszek, J. L. et al. A small molecule targeting mutagenic translesion synthesis improves chemotherapy. *Cell* **178**, 152–159. e111 (2019).
51. Chatterjee, N. et al. A stapled POL κ peptide targets REV1 to inhibit mutagenic translesion synthesis. *Environ. Mol. Mutagen.* **61**, 830–836 (2020).
52. Mentegari, E. et al. Ribonucleotide incorporation by human DNA polymerase η impacts translesion synthesis and RNase H2 activity. *Nucleic Acids Res.* **45**, 2600–2614 (2017).
53. Donigan, K. A., McLenigan, M. P., Yang, W., Goodman, M. F. & Woodgate, R. The steric gate of DNA polymerase ϵ regulates ribonucleotide incorporation and deoxyribonucleotide fidelity. *J. Biol. Chem.* **289**, 9136–9145 (2014).
54. Hiller, B. et al. Mammalian RNase H2 removes ribonucleotides from DNA to maintain genome integrity. In vivo function of mammalian RNase H2. *J. Exp. Med.* **209**, 1419–1426 (2012).
55. Sparks, J. L. et al. RNase H2-initiated ribonucleotide excision repair. *Mol. Cell* **47**, 980–986 (2012).
56. Bubeck, D. et al. PCNA directs type 2 RNase H activity on DNA replication and repair substrates. *Nucleic Acids Res.* **39**, 3652–3666 (2011).
57. Chon, H. et al. Contributions of the two accessory subunits, RNASEH2B and RNASEH2C, to the activity and properties of the human RNase H2 complex. *Nucleic Acids Res.* **37**, 96–110 (2009).
58. Adams, P. D. et al. PHENIX: a comprehensive Python-based system for macromolecular structure solution. *Acta Crystallogr. Sect. D: Biol. Crystallogr.* **66**, 213–221 (2010).
59. Emsley, P. & Cowtan, K. Coot: model-building tools for molecular graphics. *Acta Crystallogr. Sect. D: Biol. Crystallogr.* **60**, 2126–2132 (2004).
60. DeLano, W. L. Pymol: An open-source molecular graphics tool. *CCP4 NewsL. protein Crystallogr.* **40**, 82–92 (2002).
61. Li, S., Olson, W. K. & Lu, X.-J. Web 3DNA 2.0 for the analysis, visualization, and modeling of 3D nucleic acid structures. *Nucleic Acids Res.* **47**, W26–W34 (2019).
62. Case, D. A. et al. AMBER 15. (University of California, San Francisco, 2015).
63. Maier, J. A. et al. ff14SB: improving the accuracy of protein side chain and backbone parameters from ff99SB. *J. Chem. theory Comput.* **11**, 3696–3713 (2015).
64. Ramanathan, A., Agarwal, P. K., Kurnikova, M. & Langmead, C. J. An online approach for mining collective behaviors from molecular dynamics simulations. *J. Comput. Biol.* **17**, 309–324 (2010).
65. Ramanathan, A., Savol, A. J., Agarwal, P. K. & Chennubhotla, C. S. Event detection and sub-state discovery from biomolecular simulations using higher-order statistics: application to enzyme adenylate kinase. *Proteins* **80**, 2536–2551 (2012).
66. Hoitsma, N. M. et al. AP-endonuclease 1 sculpts DNA through an anchoring tyrosine residue on the DNA intercalating loop. *Nucleic Acids Res.* **48**, 7345–7355 (2020).
67. Narayanan, C. et al. Conservation of dynamics associated with biological function in an enzyme superfamily. *Structure* **26**, 426–436.e423 (2018).
68. Ramanathan, A. & Agarwal, P. K. Evolutionarily conserved linkage between enzyme fold, flexibility, and catalysis. *PLoS Biol.* **9**, e1001193 (2011).
69. Duff, M. R. Jr. et al. Modulating enzyme activity by altering protein dynamics with solvent. *Biochemistry* **57**, 4263–4275 (2018).
70. Beck, D. A. & Daggett, V. Methods for molecular dynamics simulations of protein folding/unfolding in solution. *Methods* **34**, 112–120 (2004).
71. Shukla, S. et al. Differential substrate recognition by maltose binding proteins influenced by structure and dynamics. *Biochemistry* **57**, 5864–5876 (2018).

Acknowledgements

We thank Dr. Nicole M. Hoitsma for helpful discussion and assistance with structural modeling. This research was supported by the National Institute of General Medical Science R35-GM128562 to B.D.F., R01-GM105978 to P.K.A., and R01-GM081433 to M.T.W.

Author contributions

T.M.W. and T.H.K. purified the Rev1 proteins. T.M.W. and T.H.K. collected X-ray crystallography datasets. T.M.W. B.D.F. processed and analyzed the X-ray crystallography datasets. T.H.C. and P.K.A. performed the MD simulations. T.M.W., T.H.C., P.K.A., and B.D.F. analyzed the data from MD simulations. T.M.W., M.T.W., P.K.A., and B.D.F. wrote the manuscript.

Competing interests

The authors declare no competing interests.

Additional information

Supplementary information The online version contains supplementary material available at <https://doi.org/10.1038/s41467-022-30577-0>.

Correspondence and requests for materials should be addressed to Pratul K. Agarwal or Bret D. Freudenthal.

Peer review information *Nature Communications* thanks the anonymous reviewers for their contribution to the peer review of this work.

Reprints and permission information is available at <http://www.nature.com/reprints>

Publisher's note Springer Nature remains neutral with regard to jurisdictional claims in published maps and institutional affiliations.



Open Access This article is licensed under a Creative Commons Attribution 4.0 International License, which permits use, sharing, adaptation, distribution and reproduction in any medium or format, as long as you give appropriate credit to the original author(s) and the source, provide a link to the Creative Commons license, and indicate if changes were made. The images or other third party material in this article are included in the article's Creative Commons license, unless indicated otherwise in a credit line to the material. If material is not included in the article's Creative Commons license and your intended use is not permitted by statutory regulation or exceeds the permitted use, you will need to obtain permission directly from the copyright holder. To view a copy of this license, visit <http://creativecommons.org/licenses/by/4.0/>.

© The Author(s) 2022